Nuclear Inst. and Methods in Physics Research B 474 (2020) 78–82

Contents lists available at ScienceDirect

Nuclear Inst. and Methods in Physics Research B

journal homepage: www.elsevier.com/locate/nimb

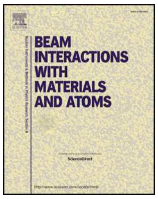

Swift heavy ion irradiation to non-amorphizable CaF_2 and amorphizable $Y_3Al_5O_{12}$ (YAG) crystals

H. Amekura[a,*], R. Li[a,b], N. Okubo[c], N. Ishikawa[c], F. Chen[b]

[a] National Institute for Materials Science (NIMS), Tsukuba, Ibaraki 305-0003, Japan
[b] School of Physics, State Key Laboratory of Crystal Materials, Shandong University, Jinan 250100, China
[c] Japan Atomic Energy Agency (JAEA), Tokai, Ibaraki 319-1195, Japan

ARTICLE INFO

Keywords:
Swift heavy ion
Non-amorphizable
CaF_2
YAG
Amorphizable

ABSTRACT

Yttrium-aluminum-garnet (YAG) and calcium fluoride (CaF_2) were irradiated with 200 MeV Xe^{14+} ions at fluences ranging from 1×10^{11} to 2×10^{14} ions/cm^2. X-ray diffraction indicated that a YAG crystal was transformed to an amorphous phase at 1×10^{13} ions/cm^2. Contrary, CaF_2 shows diffraction peaks up to the highest fluence performed of 2×10^{14} ions/cm^2, indicating the non-amorphizable nature. In spite of amorphization, YAG maintained the transparency of $>$ 80% from 500 nm to 2500 nm up to the highest fluence of 2×10^{14} ions/cm^2. Contrary, CaF_2 showed a broad absorption band centered at 550 nm even at the lowest fluence of 1×10^{11} ions/cm^2, which is ascribed to metallic Ca colloids in CaF_2. While the absorption intensity saturated around 1×10^{13} ions/cm^2, it does not mean the total metallization of the irradiated region but a dynamical equilibrium between the metallization and recovery.

1. Introduction

Swift heavy ions (SHIs) are high energy ions whose energy loss processes in solids are mostly governed by electronic friction [1]. When a SHI goes through a crystal, a damage region of cylindrical shape is formed along the ion trajectory in many insulators [2,3]. The region is called (latent) ion track, which is amorphous in many crystals but crystalline in some crystals such as CaF_2 [4], SrF_2 [4], BaF_2 [4], CeO_2 [5,6], and more. High resolution transmission electron microscopy (TEM) observations confirmed certain density reduction in the track regions in CeO_2 [6,7] and $MgAl_2O_3$ [8], mainly due to loss of the anions. In CaF_2, huge loss of F ions in the track regions result in anion-void sublattice and remaining Ca sublattice, which is observed as metallic Ca colloids in CaF_2 [9].

Another remarkable observations, which were confirmed in CeO_2 [7] and $MgAl_2O_3$ [8], are that a newly formed track erases the tracks previously formed if the distance is nearer than a certain value [10]. Consequently, the number density of the tracks saturates to a constant value at high fluences: While increasing the fluence further, the number of the tracks does not increase. This is a consequence of the dynamical equilibrium between the track generation at the center of a new impact of SHI and the track erasing at the periphery of the tracks. The track erasing could be damage recovery meditated by recrystallization.

Consequently, we expected higher radiation hardness in non-amorphizable materials than amorphizable ones. It is known that yttrium aluminum garnet (YAG; $Y_3Al_5O_{12}$) crystals are amorphized by SHI irradiation [11] with the threshold S_e of 7.5 keV/nm [12]. Contrary, it is known that CaF_2 crystals are not amorphized under SHI irradiation, while ion tracks of a crystalline phase are registered [4] with the two-step thresholds of 5 and 18 keV/nm [13]. In this paper, a comparative study between non-amorphizable CaF_2 and amophizable YAG is described against the responses to 200 MeV Xe^{14+} ion irradiation. In spite of the expectation described above, better and more stable optical transparency was observed in amorphizable YAG than non-amorphizable CaF_2. Irrespective of the amorphization, the optical transparency in the visible and the near-infrared (NIR) regions maintained in YAG. Contrary, a strong absorption over the visible and the NIR regions strongly degraded the optical transparency of CaF_2 because metallic Ca collides are generated by SHI irradiation

2. Experimental

Single-crystals of non-doped YAG and of CaF_2 with sizes of $10 \times 10 \times 1$ mm^3 were purchased from ATOM Optics Co., Ltd., China. While both the samples were single crystals in unirradiated state, they seemed to transform to polycrystalline for CaF_2 and polycrystalline and finally to amorphous for YAG, with irradiation. Here the “undoped YAG” means that Nd ions or other rare-earth impurities have not

---

* Corresponding author.
E-mail address: amekura.hiroshi@nims.go.jp (H. Amekura).

https://doi.org/10.1016/j.nimb.2020.04.023
Received 12 March 2020; Received in revised form 17 April 2020; Accepted 20 April 2020

Table 1
Electronic and nuclear stopping powers (at the surface), and the projected range of 200 MeV ^{136}Xe ions in YAG and CaF_2 crystals, calculated by SRIM 2013 [15]. Also the track formation threshold values and the X-ray penetration depths of Cr K-α line are shown.

	YAG	CaF_2
Electronic stopping power (keV/nm)	24.3	20.3
Nuclear stopping power (keV/nm)	0.091	0.069
Projected Range (μm)	13.2	16.7
Mass density (g/cm^3)	4.56	3.18
Track formation threshold (keV/nm) [16]	7.5	5
X-ray penetration depth of Cr K-α line at 15° incidence (μm) [17]	2.76	2.88

intentionally been doped. See Ref. [14] for the optical absorption changes of Nd-doped YAG crystals induced by high energy ion irradiation. The crystalline structures of YAG and CaF_2 are the garnet type and the fluorite type, respectively, while both are in the cubic symmetry. The {0 0 1} planes of both the single crystals were irradiated at room temperature with 200 MeV $^{136}Xe^{14+}$ ions from the tandem accelerator in the Japan Atomic energy Agency (JAEA), Tokai Research and Development Center. The fluence ranged from 1 × 10^{11} to 2 × 10^{14} ions/cm^2. The stopping powers and the projected ranges of the 200 MeV Xe ions in either of YAG and CaF_2 were calculated using SRIM 2013 code [15] and shown in Table 1. The Xe ion provides the electronic stopping powers S_e of 24.3 and 20.3 keV/nm in YAG and CaF_2, respectively, either of the S_e was much higher than the track formation threshold of 7.5 (YAG) and 5 keV/nm (CaF_2) [16].

The fixed incident angle X-ray diffractometry (FIA-XRD) was applied with a fixed incident angle of 15° from the sample surface using the Cr Kα line (λ = 0.22896 nm) from an X-ray source (Rigaku Co., Ltd. RINT 2500 MDG). Different from the conventional θ-2θ method, the penetration depth of the X-ray is constant for FIA-XRD irrespective of the scattering angle 2θ. Since the ion irradiation effects may depend on the sample depth, the FIA method could be advantageous. The incident angle of 15° corresponds to the X-ray penetration depth of 2.76 μm normal from the surface for YAG (the density of 4.56 g/cm^3) and 2.88 μm for CaF_2 (3.18 g/cm^3) [17]. Here the penetration depth means the depth where the incident X-ray intensity decreases to e^{-1}. The penetration depths of both the materials were much shorter than the ion range of 200 MeV Xe^{14+} ions (13.2 μm for YAG and 16.7 μm for CaF_2), indicating that the XRD signal was detected in the region where the electronic stopping is almost constant along the depth. A conventional dual-beam spectrophotometer (JASCO corp., V-670) was used for optical transmission spectroscopy in the wavelength region λ = 190–2500 nm with a resolution of 2 nm for λ < 850 nm and 8 nm for λ > 850 nm [18].

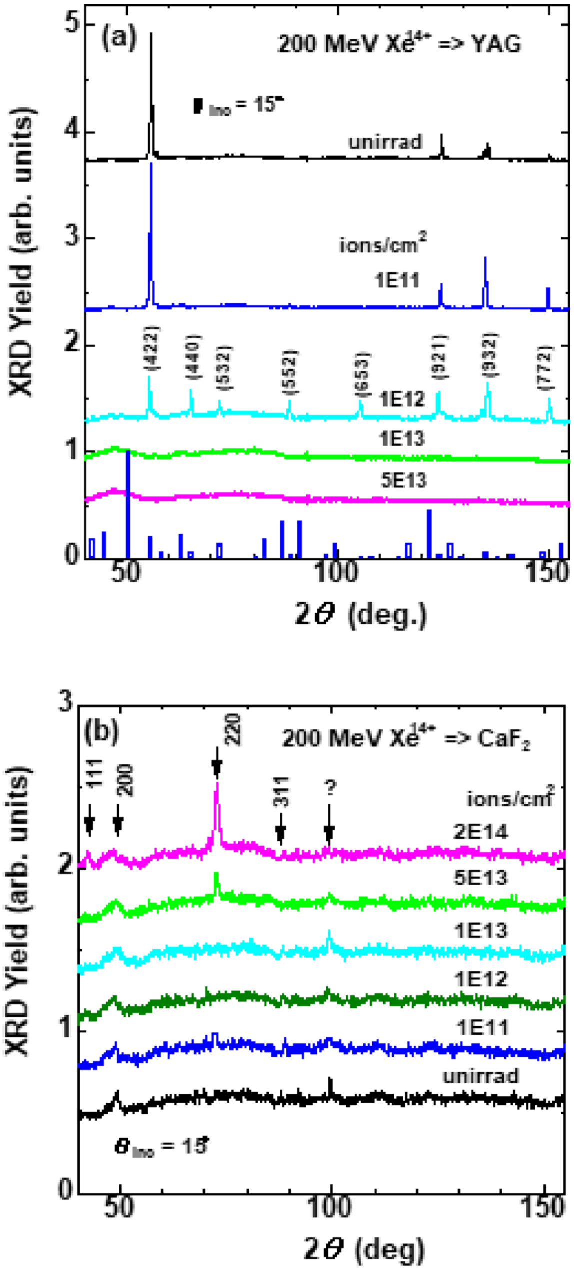

Fig. 1. Fixed-incident-angle X-ray diffraction (FIA-XRD) patterns of (a) undoped YAG and (b) CaF_2 crystals unirradiated and irradiated with 200 MeV Xe^{14+} ions to various fluences ranging from 1 × 10^{11} to 2 × 10^{14} ions/cm^2. The patterns are shifted for vertical direction for clarity. In (a), a powder diffraction pattern from literature is plotted by rectangles.

3. Results and discussion

3.1. X-ray diffraction

Fig. 1(a) exhibits FIA-XRD patterns from undoped YAG crystals irradiated with 200 MeV Xe ions to various fluences ranging from 0 to 5 × 10^{13} ions/cm^2. Since the pattern at 2 × 10^{14} ions/cm^2 was almost the same as 5 × 10^{13} ions/cm^2, it was not plotted. Before the irradiation, relatively strong four peaks were observed, which were assigned to diffractions from the garnet structure: 55.8° for (4 2 2), 124.6° for (9 2 1), 135.7° for (9 3 2), and 150.3°for (7 7 2). The powder diffraction pattern from Ref. [19] is shown in Fig. 1(a) as rectangles. Because the garnet structure includes many atoms in a unit cell, many diffraction peaks are observed in the powder pattern. However, our samples showed only limited peaks due to high crystallinity. After the irradiation to 1 × 10^{11} ions/cm^2, the same peaks were observed, while the intensity ratios and the diffraction angles slightly changed. At the fluence of 1 × 10^{12} ions/cm^2, new four peaks were added, which were also assigned to the garnet structure: 65.1° to (4 4 0), 72.0° to (5 3 2), 88.6° to (5 5 2), and 105.2° to (6 5 3). Because of the partial amorphization, the single crystal was partly broken down to grains, i.e., poly-crystallization. Consequently, the new peaks were allowed to be observed. At the fluence of 1 × 10^{13} ions/cm^2, all the diffraction peaks disappeared indicating the full amorphization of the YAG crystal. Amorphization of Nd-doped YAG crystals was already reported by RBS-Channeling [12] and TEM [5]. While it is not exactly YAG ($Y_3Al_5O_{12}$), detailed study has been carried out on YIG ($Y_3Fe_5O_{12}$) [20]. Further irradiation to 5 × 10^{13} ions/cm^2 and 2 × 10^{14} ions/cm^2 (not shown) did not induce reappearance of the peaks. The fluence dependence of the (4 2 2) diffraction yield (2θ = 55.8°) is plotted in Fig. 2(a). The amorphization at 1 × 10^{13} ions/cm^2 is clearly shown. With fitting the fluence Φ dependence of the (4 2 2) diffraction yield I by the following

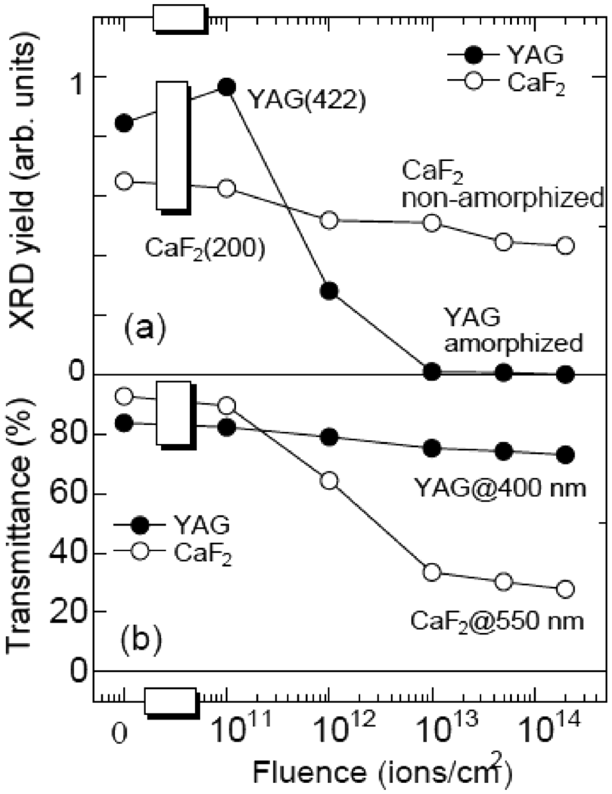

Fig. 2. (a) Fluence dependence of FIA-XRD yield of YAG (4 2 2) peak and of CaF_2 (2 0 0) peak under 200 MeV Xe^{14+} ion irradiation. (b) Fluence dependence of the optical transmittance of YAG samples at the wavelength of 400 nm and of CaF_2 samples at 550 nm (due to metallic Ca collides).

equation,

$$I(\Phi) = I_o \exp(-\pi R_{YAG}^2 \Phi) \tag{1}$$

The track radius R_{YAG} of 4.3 nm was determined. According to a relationship determined by Meftah, et al. [12] between S_e and track radius in YAG for the ion velocity of 1.24 MeV/u, the 200 MeV ^{136}Xe ion (S_e = 24.3 keV/nm, 1.47 MeV/u) is expected to generate the track of 4.2 nm in radius, which is a good agreement with the observation.

Fig. 1(b) exhibits the FIA-XRD patterns of CaF_2 crystals irradiated with 200 MeV Xe ions to various fluences ranging from 0 to 2 × 10^{14} ions/cm^2. In unirradiated state, the (2 0 0) peak was observed. (Another peak was observed at ~ 100°, which was not able to be assigned to the cubic CaF_2.) This fact indicates that the sample was oriented to (2 0 0) before the irradiation. The fluence dependence of the CaF_2 (2 0 0) diffraction yield is plotted in Fig. 2(a), which shows very slow decay with the fluence.

While the (2 0 0) peak was observed irrespective of the fluence, other peaks (1 1 1), (2 2 0), and (3 1 1) were observed at some fluences only, which could be temporarily formed from the destruction of the (2 0 0) orientation by the irradiation. However, further irradiation again transformed the temporary formed grains to the original orientations. While the pattern changed with the fluence, the changes were not systematic except the (2 0 0) peak as shown in Fig. 2(a). We rather interpret that the patterns of CaF_2 samples shown in Fig. 1(b) did not significantly change even increasing the fluence up to 2 × 10^{14} ions/cm^2, which is strong contrast with YAG samples where abrupt disappearance of the diffraction pattern was observed at 1 × 10^{13} ions/cm^2 due to amorphization. This is a marked difference between CaF_2 and YAG, and indicates a typical character of CaF_2 as a non-amorphizable crystal [13].

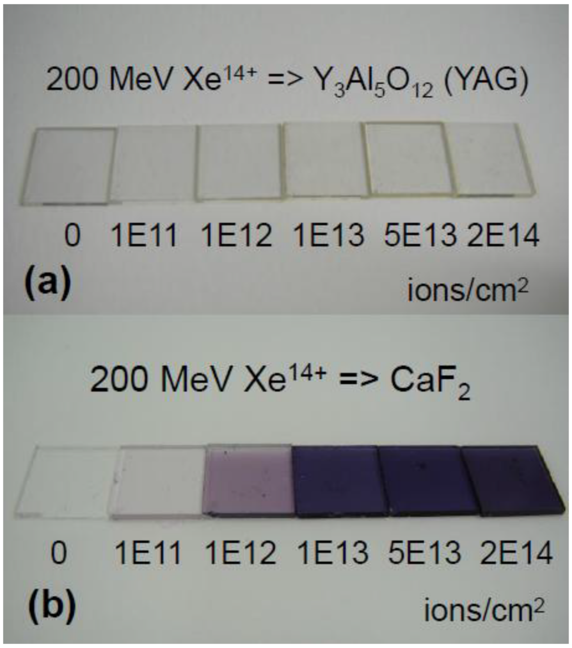

Fig. 3. Photo-images of (a) undoped YAG samples and of (b) CaF_2 samples irradiated with 200 MeV Xe^{14+} ions to various fluences from 0 to 2 × 10^{14} ions/cm^2.

3.2. Optical absorption

Color changes in YAG and in CaF_2 with the irradiation are shown as photo-images in Fig. 3 and as optical transmission spectra in Fig. 4. Both the materials showed higher transmittance than 80% in unirradiated state from the longest wavelength detected of 2500 nm to 294 nm (for YAG) and from 2500 nm to the shortest wavelength detected of 190 nm (for CaF_2). Even irradiated with 200 MeV Xe ions, YAG maintained the transparency in the visible region up to the highest fluence of 2 × 10^{14} ions/cm^2 as exhibited in the photo-image (Fig. 3(a)). While the amorphization in YAG has completed at 1 × 10^{13} ions/cm^2, little color change has been induced via the amorphization. The detailed transparency changes in YAG are shown in Fig. 4(a). With increasing the fluence, the transmission limit of 80% at the short wavelength side shifted from 294 nm (in unirradiated state) to 460 nm (at 5 × 10^{13} ions/cm^2). Once, however, the amorphization has been completed, no further shift was induced even with increasing the fluence further. The fluence dependence of the optical transmittance of YAG at 400 nm in wavelength is shown in Fig. 2(b), which indicates that high transparency is maintained irrespective of the amorphization at 1 × 10^{13} ions/cm^2.

Contrary, CaF_2 turned from transparent to violet under the irradiation even at the lowest fluence of 1 × 10^{11} ions/cm^2, as shown in the photo-image (Fig. 3(b)). The corresponding optical transmission spectra are exhibited in Fig. 4(b). With increasing the fluence up to 1 × 10^{13} ions/cm^2, a broad absorption band centered at ~ 550 nm appeared and increased. A similar absorption band was observed under 217 MeV ^{16}O irradiation to 0.17–2.0 × 10^{14} ions/cm^2 [21]. The band is ascribed to the formation of metallic Ca collides [21–23]. Additionally a shoulder is visible at ~ 380 nm, which could be ascribed to F centers [24], i.e., the point defect absorption, of CaF_2.

The colloid formation is assumed following processes [9]: First, the SHI irradiation introduces high concentration of F anion vacancies and aggregates (anion voids) along the tracks. Loss of F atoms from the CaF_2 lattice is induced on the anion sublattice, i.e., the formation of void sublattice, which is nearly independent from the Ca cation sublattice. The remaining Ca sublattice behaves as metallic collides or metal NPs embedded in CaF_2. The absorption band at ~ 550 nm is ascribed to the

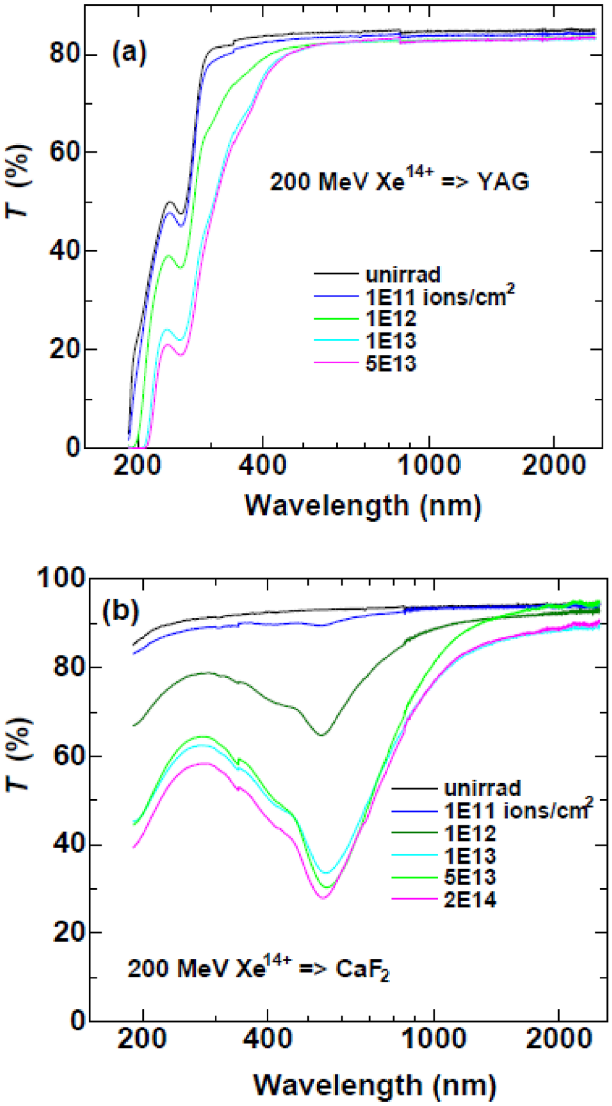

Fig. 4. Optical transmission spectra of (a) YAG and of (b) CaF_2 irradiated with 200 MeV Xe^{14+} ions to various fluences ranging from 0 to 2 × 10^{14} ions/cm^2. The abscissa (wavelength) is plotted in a logarithmic scale.

surface plasmon resonance (SPR) of metallic Ca NPs in CaF_2. However, recent scanning TEM electron energy loss spectroscopy (STEM-EELS) showed that tracks consist of rows of nano-voids where lower Ca signal and higher F signal were detected [28]. Consistency between the present story and the recent new observations is discussion in 3.4

Fluence dependence of the optical transmittance at the SPR wavelength of 550 nm is shown in Fig. 2(b). While the transmittance at 550 nm decreases with the fluence up to 1 × 10^{13} ions/cm^2, the transmittance saturates with exceeding 1 × 10^{13} ions/cm^2. The fluence dependence of the transmittance at 550 nm was fitted by following equation:

$$T_{550}(\Phi) = \{T_{550}(0) - T_{550}(\infty)\}\exp(-\pi R_{CaF2}^2\Phi) + T_{550}(\infty) \qquad (2)$$

The radius of the modified zone in CaF_2 was determined as R_{CaF2} = 2.6 nm.

The saturation behavior could be related to a fact that whole the irradiated surface of the sample was fully covered by the tracks at the fluence of ~ 1 × 10^{13} ions/cm^2. While the absorption intensity saturated at higher than 1 × 10^{13} ions/cm^2, it does not mean the total metallization of the irradiated region but the existence of dynamical equilibrium between the metallization and recovery processes.

As described in Introduction, the dynamical equilibrium was observed between the track formation and erasing in $MgAl_2O_3$ [8] and CeO_2 [7]: A newly formed track erases the tracks previously formed, if the distance is nearer than a certain value [10]. Consequently, the number density of the tracks saturates to a constant value, while the tracks are not overlapped. While increasing the fluence, the number of the tracks does not increase at high fluences. This is a consequence of the dynamical equilibrium between the track generation at the center of a new impact of SHI and the track erasing at the periphery of the newly formed track. This model is also supported by an observation that the shape of the saturated absorption band is similar with those at lower fluences, all of which are well described by Mie theory. This observation indicates that Ca collides are still embedded in dielectrics CaF_2 even at the highest fluence. The CaF_2 is still survived in the irradiated region even after the saturation.

3.3. Optical communication bands at NIR

It should be noted that the optical transmission spectra of YAG in the wavelength region between 1000 and 2000 nm are flat and almost independent of the fluence of the SHI irradiation as shown in Fig. 4(a). This is an attractive property of YAG applying for the NIR optical communication bands. Contrary, the spectra of CaF_2 in the same region changed with the fluence as shown in Fig. 4(b), which is not good for the application of CaF_2 for the NIR optical communication bands.

We expected that non-amorphizable material CaF_2 could show better optical stability against the SHI irradiation, because CaF_2 is not suffered by amorphization. The crystallinity is maintained even after high fluence irradiation. However, the point defect formation resulted in the Ca colloid formation, which degraded the optical transparency. Contrary, YAG is amorphized by the SHI irradiation at relatively low fluence of 1 × 10^{13} ions/cm^2. The optical transmission was not changed by the amorphization except the small red shift of the short wavelength transparency limit.

Therefore, comparing the optical transparency against SHI irradiation between YAG and CaF_2, the amorphizable YAG crystals is better than the non-amorphizable CaF_2 crystals.

3.4. Relationship with other observations

While we presumed that the origin of the absorption band at ~ 550 nm in CaF_2 as the metallic Ca collides, another candidate is M-centers, i.e., dimers of F-centers [25,26]. Cooke and Bennett observed a series of absorption peaks at 320, 376, 535, and 670 nm in CaF_2 irradiated with X-rays, and attributed to V_K-, F-, M-, and R-centers, respectively, probably from an analogy to alkali halides [25,26]. In our samples irradiated with 200 MeV Xe ions, only the strong and broader peak was observed at ~ 550 nm with a weak shoulder at ~ 380 nm. The peaks attributed to V_K- and R- centers are not observed. Furthermore, the ~ 550 nm peak observed under SHI irradiation was broader than that observed under the X-ray irradiation.

The formation of the Ca collides has been confirmed by TEM after the irradiations of electrons [27] and cluster ions [9]. The absorption peak at ~ 550 nm is well reproduced by Mie theory [23]. We consider that the Ca collides are more plausible explanation at the moment.

Even presuming the M-center model, the saturation of the absorption at high fluences is explained by the same model, i.e., the dynamical equilibrium between the track formation and track erasing.

Recently, STEM-EELS [28] showed that tracks consist of rows of nano-voids where lower Ca signal and higher F signal were detected, indicating that maybe F atoms were trapped there. Furthermore, in-situ time-of-flight elastic recoil detection analysis (TOF-ERDA) [28] and RBS [29] revealed that the surface composition ratio of F/Ca did not depend on the irradiation fluence. The conventional idea of the fluorine loss form the sample was excluded. However, the dissolution of CaF_2 to Ca and F is firmly evident. The mystery could be solved if we assume that the dissociated F atoms do not migrate long distance but are trapped at sites not so far away from the original positions. The dissociated Ca atoms stay with forming the collides.

4. Conclusions

Both YAG and CaF_2 were irradiated with 200 MeV Xe^{14+} ions in the fluence region between 1×10^{11} and 2×10^{14} ions/cm^2 at nominally room temperature. FIA-XRD indicated that YAG single crystal was divided into misaligned grains at 1×10^{12} ions/cm^2. Then it was amorphized at 1×10^{13} ions/cm^2 while CaF_2 maintained the crystallinity up to the highest fluence performed of 2×10^{14} ions/cm^2. This is because CaF_2 is known as a non-amorphizable material against SHI irradiation. While CaF_2 does not show the amorphization, the point defect formation by SHI irradiation resulted in the metallic Ca colloid formation, which show a strong absorption band at ~ 550 nm in the visible region. While the optical transmittance at 550 nm saturated at the fluence of 1×10^{13} ions/cm^2, it does not attributed to the total metallization of the irradiated region, but rather to the dynamical equilibrium between the track formation and track erasing. The shapes of the 550 nm band were similar irrespective of the saturation, indicating that always Ca collides are embedded in CaF_2, not Ca metal. Contrary, unrecognizable color change, except small red shift of the absorption tail, is induced in YAG even through the amorphization. In the optical communication bands (1–2 μm), transmission change is not induced in YAG, but in CaF_2. Comparing with the optical transparency change between YAG and CaF_2 against SHI irradiation, the amorphizable YAG crystals is better than the non-amorphizable CaF_2 crystals.

Declaration of Competing Interest

The authors declare that they have no known competing financial interests or personal relationships that could have appeared to influence the work reported in this paper.

Acknowledgments

A part of the study was supported by the Inter-organizational Atomic Energy Research Program through an academic collaborative agreement among JAEA, QST, and the Univ. of Tokyo. Also the other part was carried out under the Common-Use Facility Program of JAEA. The authors are grateful to the staff of the accelerator facility at JAEA-Tokai for their help. This study was supported by JSPS-KAKENHI Grant Number 18K04898. The authors thank China Scholarship Council for supporting RL to stay for one year in NIMS, Japan.

References

[1] D.K. Avasthi and G.K. Mehta, Swift Heavy Ions for Materials Engineering and Nanostructuring, Vol. 145 (2011).
[2] D.A. Young, Etching of Radiation Damage in Lithium Fluoride, Nature 182 (1958) 375.
[3] E.C.H. Silk, R.S. Barnes, Examination of fission fragment tracks with an electron microscope, Phil. Mag. 4 (1959) 970.
[4] N. Ishikawa, T. Taguchi, N. Okubo, Hillocks created for amorphizable and non-amorphizable ceramics irradiated with swift heavy ions, TEM Sudy Nanotechnol. 28 (2017) 445708.
[5] N. Ishikawa, N. Okubo, T. Taguchi, Experimental evidence of crystalline hillocks created by irradiation of CeO_2 with swift heavy ions, TEM study Nanotechnol. 26 (2015) 355701.
[6] S. Takaki, K. Yasuda, T. Yamamoto, S. Matsumura, N. Ishikawa, Atomic structure of ion tracks in Ceria, Nucl. Instrum. Methods Phys. Res., Sect. B 326 (2014) 140.
[7] S. Takaki, K. Yasuda, T. Yamamoto, S. Matsumura, N. Ishikawa, Structure of ion tracks in ceria irradiated with high energy xenon ions, Prog. Nucl. Energy 92 (2016) 306.
[8] K. Yasuda, T. Yamamoto, M. Etoh, S. Kawasoe, S. Matsumura, N. Ishikawa, Accumulation of radiation damage and disordering in $MgAl_2O_4$ under swift heavy ion irradiation, Int. J. Mater. Res. 102 (2011) 1082.
[9] J. Jensen, A. Dunlop, S. Della-Negra, Tracks induced in CaF_2 by MeV cluster irradiation, Nucl. Instrum. Methods Phys. Res., Sect. B 141 (1998) 753.
[10] H. Amekura, N. Okubo, F. Ren, N. Ishikawa, Swift heavy ion irradiation to ZnO nanoparticles: Steep degradation at low fluences and stable tolerance at high fluences, J. Appl. Phys. 124 (2018) 145901.
[11] M.D. Rodriguez, W.X. Li, F. Chen, C. Trautmann, T. Bierschenk, B. Afra, D. Schauries, R.C. Ewing, S.T. Mudie, P. Kluth, SAXS and TEM investigation of ion tracks in neodymium-doped yttrium aluminium garnet, Nucl. Instrum. Methods Phys. Res., Sect. B 326 (2014) 150.
[12] A. Meftah, M. Djebara, N. Khalfaoui, J.P. Stoquert, F. Studer, M. Toulemonde, Thermal Spike Description of the Damage Creation in $Y_3Al_5O_{12}$ Induced by Swift Heavy Ions, Mater. Sci. Forum (Proc. of ICDS-18) 248–249 (1997) 53.
[13] M. Toulemonde, A. Benyagoub, C. Trautmann, N. Khalfaoui, M. Boccanfuso, C. Dufour, F. Gourbilleau, J.J. Grob, J.P. Stoquert, J.M. Costantini, F. Haas, E. Jacquet, K.O. Voss, A. Meftah, Dense and nanometric electronic excitations induced by swift heavy ions in an ionic CaF_2 crystal: Evidence for two thresholds of damage creation, Phys. Rev. B 85 (2012) 054112.
[14] H. Amekura, S. Akhmadaliev, S. Zhou, F. Chen, A possible new origin of long absorption tail in Nd-doped yttrium aluminum garnet induced by 15 MeV gold-ion irradiation and heat treatment, J. Appl. Phys. 119 (2016) 173104.
[15] J.F. Ziegler, J.P. Biersack, M.D. Ziegler, SRIM - The Stopping and Range of Ions in Matter, SRIM Co., Maryland, 2008.
[16] N. Itoh, D.M. Duffy, S. Khakshouri, A.M. Stoneham, Making tracks: electronic excitation roles in forming swift heavy ion tracks, J. Phys.: Condens. Matter 21 (2009) 474205.
[17] The Center for X-ray Optics, X-ray Database, Lawrence Berkeley National Laboratory http://henke.lbl.gov/optical_constants/.
[18] H. Amekura, Ultraviolet–Visible Spectrophotometry, in Compendium of Surface and Interface Analysis, edited by The Surface Science Society of Japan (Springer Singapore, Singapore, 2018), p. 791.
[19] K.L. Ovanesyan, A.G. Petrosyan, G.O. Shirinyan, A.A. Avetisyan, Optical dispersion and thermal expansion of garnets $Lu_3Al_5O_{12}$, $Er_3Al_5O_{12}$, and $Y_3Al_5O_{12}$, Inorg. Mater. 17 (1981) 308.
[20] A. Meftah, F. Brisard, J.M. Costantini, M. Hage-Ali, J.P. Stoquert, F. Studer, M. Toulemonde, Swift heavy ions in magnetic insulators: A damage-cross-section velocity effect, Phys. Rev. B 48 (1993) 920.
[21] M. Boccanfuso, A. Benyagoub, K. Schwartz, C. Trautmann, M. Toulemonde, Study of the damage produced in CaF_2 by swift heavy ion irradiation, Nucl. Instrum. Methods Phys. Res., Sect. B 191 (2002) 301.
[22] J. Jensen, A. Dunlop, S. Della-Negra, Microscopic observations of metallic inclusions generated along the path of MeV clusters in CaF_2, Nucl. Instrum. Methods Phys. Res., Sect. B 146 (1998) 399.
[23] V.M. Orera, E. Alcalá, Optical properties of cation colloidal particles in CaF_2 and SrF_2, Phys. Status Solidi (a) 44 (1977) 717.
[24] T. Kamikawa, Y. Kazumata, A. Kikuchi, K. Ozawa, The F center in calcium fluoride, Phys. Lett. 21 (1966) 126.
[25] D.W. Cooke, B.L. Bennett, Optical absorption and luminescence of 14 MeV neutron-irradiated CaF_2 single crystals, J. Nucl. Mater. 321 (2003) 158.
[26] C. Pandurangappa, B.N. Lakshminarasappa, F. Singh, K.R. Nagabhushana, Optical absorption and thermoluminescence studies in 100MeV swift heavy ion irradiated CaF_2 crystals, Nucl. Instrum. Methods Phys. Res., Sect. B 269 (2011) 185.
[27] E. Johnson, L.T. Chadderton, Anion voidage and the void superlattice in electron irradiated Caf2, Radiat. Effects 79 (1983) 183.
[28] M. Karlušić, C. Ghica, R.F. Negrea, Z. Siketić, M. Jakšić, M. Schleberger, S. Fazinić, On the threshold for ion track formation in CaF_2, New J. Phys. 19 (2017) 023023.
[29] R.K. Pandey, M. Kumar, S.A. Khan, T. Kumar, A. Tripathi, D.K. Avasthi, A.C. Pandey, Study of electronic sputtering of CaF_2 thin films, Appl. Surf. Sci. 289 (2014) 77.